ELSEVIER

Recombination rates in heterojunction silicon solar cells analyzed by impedance spectroscopy at forward bias and under illumination

Ivan Mora-Seró[a], Yan Luo[a], Germà Garcia-Belmonte[a,*], Juan Bisquert[a], Delfina Muñoz[b], Cristóbal Voz[b], Joaquim Puigdollers[b], Ramon Alcubilla[b]

[a]*Departament de Física, Universitat Jaume I, E-12071 Castelló, Spain*
[b]*Departament d'Enginyeria Electrònica, Universitat Politècnica de Catalunya, E-08034 Barcelona, Spain*

Abstract

Impedance spectroscopy (at forward bias and under illumination) of solar cells comprised thin hydrogenated amorphous silicon (a-Si:H) films deposited on crystalline silicon (c-Si) wafers was analyzed in terms of ac equivalent circuits. Shockley–Read–Hall recombination at states on the device interfaces governs the cell dynamic response. Recombination process was modeled by means of simple RC circuits which allow to determine the capture rate of electrons and holes. Carrier lifetime is found to be stated by the electron capture time $\tau_{SRH} \approx \tau_n$, and it results in the range of 300 μs. The Al-annealed back contact was regarded as the dominating recombination interface.
© 2007 Elsevier B.V. All rights reserved.

1. Introduction

Heterojunction solar cells with thin hydrogenated amorphous silicon (a-Si:H) films deposited on crystalline silicon (c-Si) wafers have attracted much attention because of their high-efficiency and low-cost fabrication process. These devices are an excellent alternative for the fabrication of high-efficiency silicon solar cells in an entirely low-temperature process. Device performance greatly depends on the a-Si:H/c-Si front interface properties, along with on the preparation procedure of the back contact. It has been seldom recognized [1] that useful knowledge may be gathered by analyzing ac characteristics of solar cells in addition to dc curves. Recently, a-Si:H/c-Si interface properties have been studied from admittance spectroscopy at zero or small reverse bias [2]. Capacitance dependence on bias and temperature has been proposed as a useful technique to obtain information on interface parameters such as the interface defect density. When solar cells are submitted at forward bias or work under illumination, the device dynamic response turns to be governed by charge accumulation and recombination mechanisms. Effective carrier lifetime τ_{eff} can be readily obtained from impedance spectra of complete cells in open-circuit conditions under varying irradiance [3]. The validity of this technique was confirmed in comparison with quasi-steady-state photo-conductance measurements. In addition, the analysis of the low-frequency capacitance at forward bias has been proposed as a characterization tool for determining interfacial a-Si:H/c-Si parameters and back-contact (annealed Al) surface recombination rate [4]. The aim of this work is the analysis of recombination processes occurring in complete solar cells of this kind by means of impedance spectroscopy.

2. ac equivalent circuit

It is widely admitted that the dominating loss mechanism in heterojunction solar cells is the so-called Shockley–Read–Hall (SRH) recombination at states on the device interfaces [5]. Recombination is then mediated by interface states, which capture both electrons and holes from

---

*Corresponding author. Tel.: +34 964 728040; fax: +34 964 729218.
E-mail address: garciag@uji.es (G. Garcia-Belmonte).

conduction and valence band, respectively [6]. The SRH carrier lifetime results by summing terms related to the capture rate of electrons and holes in the recombination centers. Occupancies of conduction band electrons, valence band holes and interface states all intervene in a dynamically complex way in the SHR recombination process. Fortunately, small signal ac circuit models corresponding to SRH recombination in steady-state conditions were proposed some decades ago by Sah and Ho Chan [7], with a high degree of generality. For fitting purposes, the general equivalent circuit should be simplified without loosing essential physics. A brief outline of a useful ac equivalent circuit of a solar cell is as follows. The capacitive effect corresponding to the excess minority carriers (C_n usually known as diffusion capacitance or chemical capacitance) [8] informs on the occupancy change of conduction band electrons [9]:

$$C_n = e^2 \frac{dn}{dE_{Fn}}. \tag{1}$$

Here the capacitance is given per unit volume. e stands for the positive elementary charge, n corresponds to the free electron concentration, and E_{Fn} accounts for the electron quasi-Fermi level. Since at forward bias or under usual illuminations, the device can work in high-injection conditions, the occupancy change of valence band holes gives rise to an additional capacitance C_p, being p the hole concentration and E_{Fp} the hole quasi-Fermi level:

$$C_p = -e^2 \frac{dp}{dE_{Fp}}. \tag{2}$$

The actual values of these two capacitances will depend on the steady-state excess carrier level, which decreases as the recombination processes go faster, and can be calculated by integration of Eqs. (1) and (2) over the absorber volume. It is expected an additional capacitive effect C_t, linked to concentration changes of occupied and empty surface recombination centers as they capture both electrons and holes. It should be stressed the different spatial origin of these three capacitive effects. While C_n and C_p mainly depends on the accumulation of excess carriers within the volume of the absorber layer, C_t has a surface origin. In addition, the depletion layer capacitance C_j, usually associated with the a-Si:H/c-Si front interface, dominates the response at low forward bias [10]. Resistive effects arise from the electron capture R_n, and similarly hole capture R_p at the recombination center in such a way that the SRH carrier lifetime results by considering separated contributions from capture times of each carrier type.

$$\tau_{SRH} = \tau_n + \tau_p = R_n C_n + R_p C_p. \tag{3}$$

An additional series resistance is needed to model contact and wire effects R_s. In the forward bias direction, the diffusion capacitances increases due to the carrier accumulation in the absorber layer and excess the junction capacitance, $C_{n,p} > C_j$ [8]. The ac equivalent circuit, which takes into account all these assumptions, is represented in Fig. 1. By recalling that C_t appears from the occupancy change of surface states (confined at the interfaces), and taking into account that it is connected in series with the rest of the circuit, it would be a good approximation to regard $C_t \gg C_{n,p}$, or equivalently to replace C_t by a short circuit (see Fig. 1(b)). Roughly speaking, this last equivalent circuit behaves like two parallel RC subcircuits in series with R_s. Therefore, one should observe two separated semicircles in a Z'–Z'' complex plane representation provided that capture times are well separated. In this derivation, we have neglected capture time distributions as expected from surface recombination centers distributed in energy within the bandgap.

3. Results and discussion

The heterojunction silicon solar cells studied in this work are obtained on p-type flat ($14\,\Omega\,cm$) CZ silicon wafers of
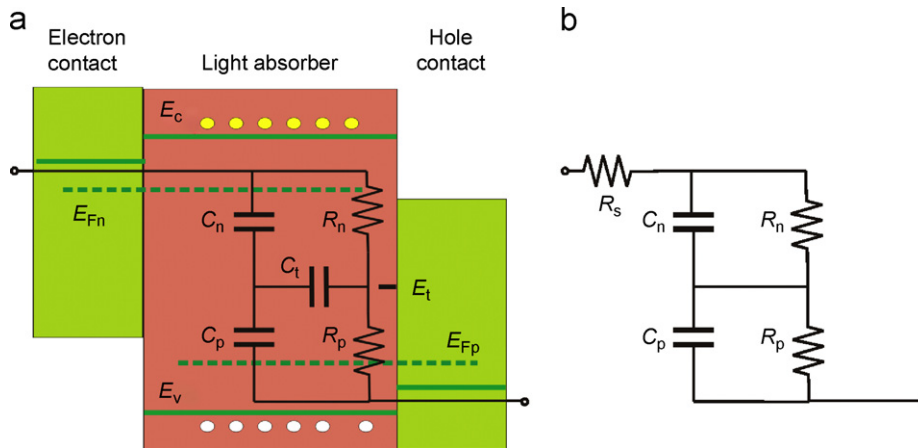

Fig. 1. (Color online) (a) Main dynamic processes occurring in the solar cell absorber layer, adapted from Ref. [7]. Modulation of accumulated excess carriers gives rise to capacitances C_n and C_p. SRH capture of conduction band electrons and valence band holes by the recombination center are modeled by resistive elements, R_n and R_p, respectively. C_t accounts for concentration changes of occupied and empty surface recombination centers. (b) Equivalent circuit used for fitting assuming $C_t \gg C_{n,p}$. An additional series resistance is needed to model contact and wire effects R_s.

Table 1
Heterostructures analyzed in this work

n-Doped	V_{oc} (mV)	J_{sc} (mA cm^{-2})	Efficiency (%)	Fill factor (%)
A a-Si:H (25 nm)	610	30.9	13.4	71.2
B a-Si:H (20 nm)	608	31.4	13.8	72.3
C a-Si:H (10 nm)	598	32.3	14.1	73.8

thickness 300 μm with aluminum back-surface-field (Al-BSF), following a method described elsewhere. The inner structure of the studied solar cells was indium tin oxide (ITO)/(n)a-Si:H/(i)a-Si:H/(p)c-Si/Al, with all the films deposited by hot-wire chemical vapor deposition technique [11]. The thickness of the intrinsic passivation a-Si:H layer was 5 nm. The solar cells are defined with an area of 4 cm^2 by sputtering 85-nm-thick ITO layers, followed by an evaporated silver grid. Efficiency around 13–14% and fill factor 71–74% were obtained depending on the thickness off the n-doped emitter (see Table 1). The J_{sc} value is slightly reduced with the thickness of the n-doped layer due to the optical absorption in the emitter, while the V_{oc} value is increased in about 12 mV. Finally, the variations in the FF value could be attributed to eventual differences in the series resistance introduced by the silver grid. The impedance measurements were carried out using an Autolab PGSTAT-30 equipped with a frequency analyzer module in the frequency range between 1 MHz and 1 Hz. Ac oscillating amplitude was as low as 10 mV (RMS) in order to maintain the linearity of the response. Impedance spectra were recorded either in the dark under varying bias voltage or in open-circuit conditions under varying illumination up to 1.5 sun (AM 1.5 Newport). This last measuring procedure was achieved by applying the bias voltage, which corresponds to V_{oc}. It yields a more homogeneous distribution of excess carriers because dc current is not allowed.

An example of the impedance spectra measured under varying irradiance and open-circuit conditions is shown in Fig. 2 (dots). One can observe two semicircles in a Z'–Z'' complex plot with decreasing size for increasing illumination. This trend is observed to be general, although at high illumination levels ($V_{oc} > 0.55$ V), only one arc appears because the high-frequency part of the spectra is masked by inductive, wire effects. The contact series resistance results approximately equal to 4 Ω cm^2. The characteristic frequency of each semicircle is interpreted in terms of the capture rate of electrons $\omega_n = \tau_n^{-1}$ and holes $\omega_p = \tau_p^{-1}$, as indicated in Fig. 2. Using standard software, fitting of the equivalent circuit model to the experimental spectra was made (solid lines in Fig. 2). Results are summarized in Fig. 3. At low bias (< 0.3 V), only one semicircle is present which accounts for the junction properties (depletion capacitance), observable in the low-bias capacitance plateau. For potentials more positive than 0.3 V, chemical electron capacitance dominates exhibiting the standard exponential dependence with bias potential U (or V_{oc}),
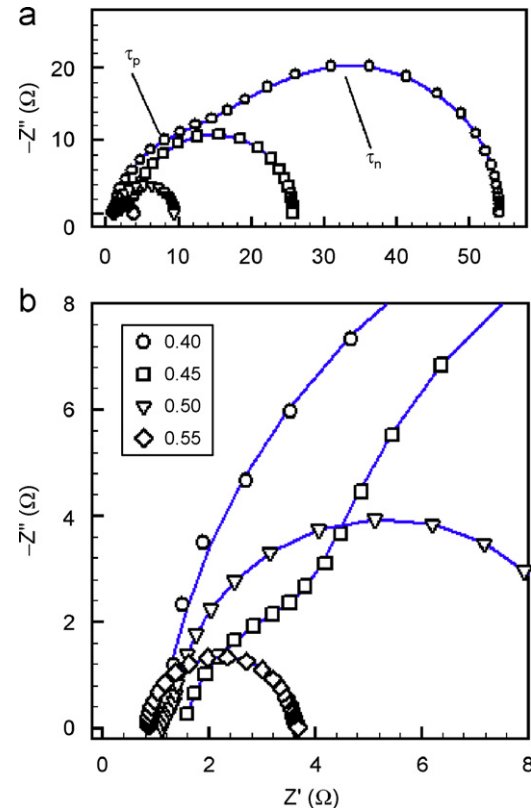

Fig. 2. (Color online) Impedance spectra measured in open-circuit conditions under varying illumination (Cell A) at room temperature. Experimental points and fitting results (solid line) using the equivalent circuit model of Fig. 1(b). Several values of the registered V_{oc} are shown. Characteristic times are marked.

$C_n \propto \exp(U/kT)$, within more than 4 orders of magnitude. C_p also shows a huge increase, which indicates the extent of the occupancy change of valence band holes. A detailed analysis of these capacitances would entail the calculation of the steady-state charge carrier density assuming the experimental conditions. An approximation may be given by regarding infinite carrier mobility (i.e. $-eV_{oc} = E_{Fn} - E_{Fp}$, which is the free energy of an electron–hole pair) and homogeneous carrier density profiles. Capacitances per unit area (L is the absorber c-Si thickness) result by considering Eqs. (1) and (2) and the carrier concentration dependence on the splitting of the quasi-Fermi levels [5]:

$$C_{n,p} = \frac{e^2 L}{2kT} \frac{n_i^2 \exp[(E_{Fn} - E_{Fp})/kT]}{\sqrt{(N_A/2)^2 + n_i^2 \exp[(E_{Fn} - E_{Fp})/kT]}}. \quad (4)$$

This expression predicts a slope change in a log C vs. V_{oc} from $1/kT$ to $1/2kT$ at injection levels corresponding to $V_{oc} \approx 0.6$ V by assuming intrinsic carrier concentration $n_i = 10^{10}$ cm^{-3}, and wafer doping $N_A = 2.0 \times 10^{15}$ cm^{-3}. This value of the wafer doping was determined using capacitance spectroscopy in reverse and low forward bias U by means of Mott–Schottky, C^{-2} vs. U analysis. Despite the approximating assumptions, capacitance variations
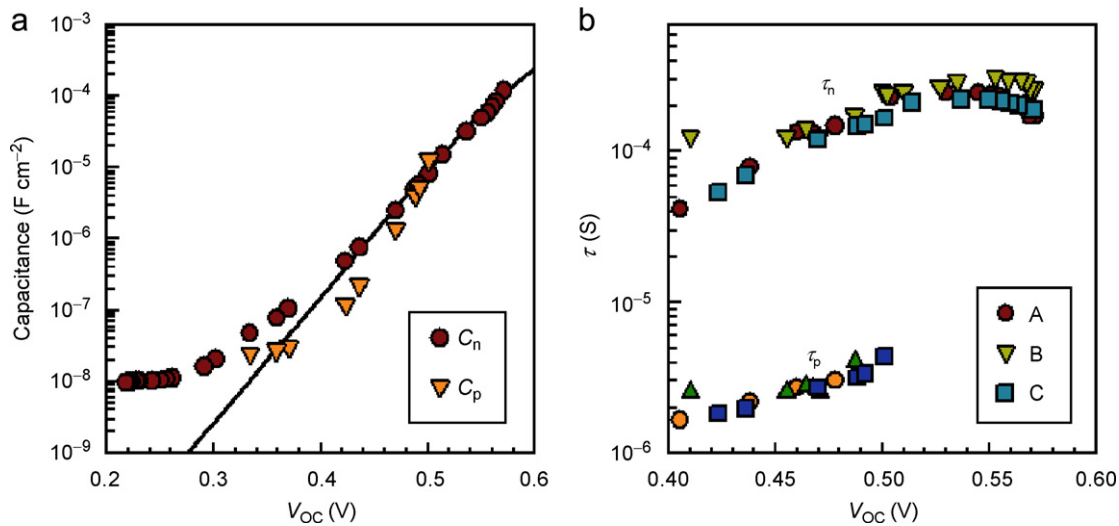
Fig. 3. (Color online) (a) Example of the electron and hole accumulation capacitances, C_n and C_p, as a function of V_{oc} for cell C. Solid line corresponds to Eq. (4) by assuming intrinsic carrier concentration $n_i = 10^{10}\,\text{cm}^{-3}$, wafer doping $N_A = 2.0 \times 10^{15}\,\text{cm}^{-3}$, and room temperature $T = 290\,\text{K}$. (b) Electron and hole capture times, τ_n and τ_p, as a function of V_{oc}.

shown in Fig. 3(a) are in good agreement with the approach of Eq. (4).

The capture times resulting from fits can be observed in Fig. 3(b). Two well-separated time constants are obtained that differ in approximately 2 orders of magnitude. Although the equivalent circuit model does not inform on the carrier type which should account for the longer (or shorter) response time, some arguments can be given that allow to ascribe longer time constants $\tau \approx 300\,\mu\text{s}$ to the electron capture process. We consider that the inclusion of the intrinsic a-Si:H buffer layer allows the passivation of the front contact in a high degree. This fact points to the Al-annealed back contact as the dominating recombination interface, as it was suggested in a previous work [12]. Since in the region near the back contact c-Si is p$^+$-doped by effect of the Al annealing, a reduction of the electron concentration is expected. Therefore, it should be electrons that determine the complete surface recombination. From Eq. (3), it is derived that the SRH carrier lifetime is dominated by the electrons $\tau_{\text{SRH}} \approx \tau_n$, which slow down the overall process of surface recombination. An estimation of the surface recombination velocity can be done by regarding the absorber thickness, and results in $S_{\text{eff}} \approx 100\,\text{cm s}^{-1}$ [13]. This value points again to the Al-BSF contact as mainly responsible for the recombination process.

Finally, capture rates as a function of temperature were calculated in the dark under application of forward bias. Fig. 4 summarizes the results for two different bias voltages. τ_p slightly decreases as the temperature increases, whereas τ_n steeply increases with temperature. Such increment in the electron lifetime is believed to be caused by the dependence of the electron capture coefficient on temperature [14]. It should be stressed that the capture times measured in the dark differ from those measured in open circuit under illumination. Electron lifetime results
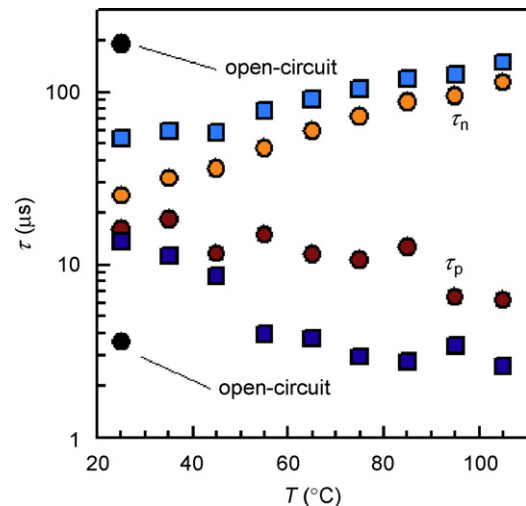

Fig. 4. (Color online) Electron and hole capture times as a function of the temperature measured in the dark under application of forward bias U (0.5 V, circles and 0.6 V, squares). Measurements done under illumination in open-circuit conditions are shown for comparison.

longer when a more homogeneous distribution of the excess carrier is reached (zero current conditions). Instead, hole capture time exhibits the opposite behavior, it is shorter in open-circuit conditions. These results might be associated with changes in the carrier concentration in the vicinity of the recombination back surface depending on the experimental conditions. A detailed study of this effect lies outside the scope of this work and it will be subject of further analysis.

Acknowledgments

References

[1] R. Anil-Kumar, M.S. Suresh, J. Nagaraju, IEEE Trans. Electron Devices 48 (2001) 2177;
G. Friesen, E.D. Dunlop, R. Wendt, Thin Solid Films 387 (2001) 239;
D. Chenvidhya, K. Kirtikara, C. Jivacete, Sol. Energy Mater. Sol. Cells 80 (2003) 459.

[2] A.S. Gudovskikh, J.P. Kleider, J. Damon-Lacoste, P. Roca i Cabarrocas, Y. Veschetti, J.C. Muller, P.J. Ribeyron, E. Rolland, Thin Solid Films 511–512 (2006) 385.

[3] G. Garcia-Belmonte, J. García-Cañadas, I. Mora-Seró, J. Bisquert, C. Voz, J. Puigdollers, R. Alcubilla, Thin Solid Films 514 (2006) 254.

[4] A.S. Gudovskikh, J.P. Kleider, Appl. Phys. Lett. 90 (2007) 034104.

[5] R. Brendel, Thin-film Crystalline Silicon Solar Cells. Physics and Technology, Wiley-VCH Verlag, Wheinheim, 2003.

[6] W. Schockley, W.T. Read, Phys. Rev. 87 (1952) 835;
R.N. Hall, Phys. Rev. 87 (1952) 387.

[7] P.C. Ho Chan, C.T. Sah, IEEE Trans. Electron Devices ED-26 (1979) 924.

[8] S.M. Sze, Physics of Semiconductor Devices, second ed., Wiley, New York, 1981.

[9] J. Bisquert, D. Cahen, G. Hodes, S. Rühle, A. Zaban, J. Phys. Chem. B 108 (2004) 8106.

[10] G. Garcia-Belmonte, J. Bisquert, V. Caselles, Solid-State Electron. 42 (6) (1998) 939.

[11] C. Voz, D. Muñoz, M. Fonrodona, I. Martin, J. Puigdollers, R. Alcubilla, J. Escarre, J. Bertomeu, J. Andreu, Thin Solid Films 511–512 (2006) 415.

[12] D. Muñoz, C. Voz, I. Martin, A. Orpella, J. Puigdollers, R. Alcubilla, F. Villar, J. Bertomeu, J. Andreu, J. Damon-Lacoste, P. Roca i Cabarrocas, Thin Solid Films, 2007, in press, doi:10.1016/j.tsf.2007.06.192.

[13] A.G. Aberle, Crystalline Silicon Solar Cells. Advanced Surface Passivation and Analysis, University of New South Wales, Sydney, 1999.

[14] N. Keskitato, P. Jonsson, K. Nordgren, H. Bleichner, E. Nordlander, J. Appl. Phys. 83 (1998) 4206.